RESEARCH ARTICLE

Rising Severe Convective Storms in the Peruvian Central Andes: Projections from Convection Permitting Regional Climate Simulations

Yongjie Huang[1] | **Ming Xue**[1,2] | **Xiao-Ming Hu**[1,2] | **Elinor Martin**[2,3] | **Héctor Mayol Novoa**[4] | **Renee A. McPherson**[3,5] | **Changhai Liu**[6] | **Mengye Chen**[1,7] | **Yang Hong**[7] | **Andres Perez**[4] | **Isaac Yanqui Morales**[4] | **José Luis Ticona Jara**[8] | **Auria Julieta Flores Luna**[4]

[1]Center for Analysis and Prediction of Storms, University of Oklahoma, Norman, OK, USA

[2]School of Meteorology, University of Oklahoma, Norman, OK, USA

[3]South Central Climate Adaptation Science Center, University of Oklahoma, Norman, OK, USA

[4]Universidad Nacional de San Agustín de Arequipa, Arequipa, Perú

[5]Department of Geography and Environmental Sustainability, University of Oklahoma, Norman, OK, USA

[6]NSF National Center for Atmospheric Research, Boulder, Colorado, USA

[7]School of Civil Engineering and Environmental Engineering, University of Oklahoma, Norman, OK, USA

[8]Servicio Nacional de Meteorología e Hidrología del Perú (SENAMHI), Arequipa, Perú

Correspondence
Yongjie Huang; Ming Xue; Hector Mayol Novoa
Email: huangynj@gmail.com; mxue@ou.edu; hnovoa@unsa.edu.pe

To explore the potential impacts of climate change on precipitation and mesoscale convective systems (MCSs) in the Peruvian Central Andes, a region with complex terrain, two future and one historical convection-permitting regional climate simulations are conducted using the Weather Research and Forecasting (WRF) model. All simulations adopt consistent model configurations and two nested domains with grid spacings of 15 and 3 km covering the entire South America and the Peruvian Central Andes, respectively. The future simulations are run for 2070–2080 and driven by a bias-corrected global dataset derived from the Coupled Model Intercomparison Project Phase 6 (CMIP6) ensemble under the SSP2-4.5 and SSP5-8.5 emission scenarios. Results show geographically dependent changes in annual precipitation, with a consistent rise in the frequency of intense hourly precipitation across all examined regions. The western Amazon Basin shows a decrease in annual precipitation, while increases exist in parts of the Peruvian west coast and the east slope of the Andes under both future scenarios. In

Funding information
Universidad Nacional de San Agustín de Arequipa (UNSA) of Peru, Grant Number: 20163646499; DOE ASR, Award Number: DE-SC0024317

the warming scenarios, there is an overall increase in the frequency, precipitation intensity, and size of MCSs east of the Andes, with MCS precipitation volume increasing by up to ~22.2%. Despite consistently enhanced synoptic-scale low-level jets in future scenarios, changes in low-level dynamic convergence are inhomogeneous and predominantly influence annual precipitation changes. The increased convective available potential energy (CAPE), convective inhibition (CIN), and precipitable water (PW) in a warming climate suppress weak convection, while fostering a more unstable and moisture-rich atmosphere facilitating more intense convection and the formation and intensification of heavy precipitation-producing MCSs. The study highlights the value of convection-permitting climate simulations in projecting future severe weather hazards and informing climate adaptation strategies, especially in regions characterized by complex terrain.

KEYWORDS
severe convective storms, future projections, convection-permitting, regional climate simulations, Peruvian Central Andes

1 | INTRODUCTION

Understanding the impacts of climate change on hydroclimatic variables is vital for a wide range of sectors, including agriculture, water resources, transportation, and disaster management (IPCC, 2021). As climate change continues to impact weather systems and water cycles, having reliable future projections is crucial for mitigating risks and ensuring sustainable development (IPCC, 2022a,b; Zaitchik et al., 2023). In this context, global climate models (GCMs) have been widely used to produce climate change projections under different scenarios at global and continental scales (O'Neill et al., 2016; Juckes et al., 2020; IPCC, 2021). However, due to constraints in computational resources the coarse spatial resolution of current GCMs (typically at grid spacings of ~100 km, Juckes et al., 2020) is a significant limitation to represent local forcings and precipitation processes (or weather conditions), particularly in regions with complex topography (Giorgi, 2019; Kendon et al., 2021; IPCC, 2021).

Regional climate modeling (i.e., dynamical downscaling) offers a temporary solution to this issue, especially when using convection-permitting models (CPMs) typically at a grid spacing of 4 km or less (Prein et al., 2015; Giorgi, 2019; Kendon et al., 2021; Lucas-Picher et al., 2021). Because CPMs have capabilities to capture local-scale forcings with a greater detail, represent local- and meso-scale dynamics, thermo- and hydro-dynamics more realistically, and resolve deep convection explicitly, their added value in simulating precipitation and mesoscale convective systems (MCSs) in different regions around the world has been highlighted by many previous studies (e.g., Prein et al., 2013; Fosser

et al., 2015; Sun et al., 2016; Gao et al., 2017; Karki et al., 2017; Kendon et al., 2017; Liu et al., 2017; Stratton et al., 2018; Zhu et al., 2018; Berthou et al., 2020; Fumière et al., 2020; Guo et al., 2020; Kouadio et al., 2020; Lind et al., 2020; Prein et al., 2020; Schumacher et al., 2020; Li et al., 2021; Halladay et al., 2023; Huang et al., 2023a,b; Paccini and Stevens, 2023). Thus, the adoption of CPMs for climate impact projections has been on the rise, particularly for examining phenomena at local and mesoscale levels (e.g., Ban et al., 2015; Liu et al., 2017; Komurcu et al., 2018; Wang and Wang, 2019; Kendon et al., 2019; Vanden Broucke et al., 2019; Chan et al., 2020; Fosser et al., 2020; Knist et al., 2020; Kurkute et al., 2020; Chapman et al., 2021; Chen et al., 2021; Ikeda et al., 2021; Qing and Wang, 2021; Ascott et al., 2023; Gensini et al., 2023; Hwang et al., 2023; Lind et al., 2023; Sonuç et al., 2023). Many CPM studies indicated that the frequency and intensity of hourly or sub-daily intense precipitation are projected to increase in different regions around the world under higher greenhouse gas emission scenarios (e.g., Ban et al., 2015; Prein et al., 2017b; Berthou et al., 2019; Kendon et al., 2019; Vanden Broucke et al., 2019; Wang and Wang, 2019; Knist et al., 2020; Chen et al., 2021; Qing and Wang, 2021; Lind et al., 2023). For example, high-resolution CPM regional climate simulations over the US, show that in a future climate under the Representative Concentration Pathways 8.5 (RCP8.5) scenario, strong convection is expected to increase at the expense of weak to moderate convection, supported by changes in convective available potential energy (CAPE) and convective inhibition (CIN), potentially impacting Earth's water and energy budgets (Rasmussen et al., 2020). Given that MCSs are significant contributors to precipitation in many regions (Salio et al., 2007; Li et al., 2020; Roca and Fiolleau, 2020; Schumacher and Rasmussen, 2020; Anselmo et al., 2021; Hu et al., 2021; Kukulies et al., 2021; Zhao, 2022; Paccini and Stevens, 2023), understanding the behavior of MCSs in CPM-based climate projections is critical to enhancing our understanding of a changing convective population and precipitation in a future climate (e.g., Prein et al., 2017a; Fitzpatrick et al., 2020; Haberlie et al., 2023; Hwang et al., 2023). Prein et al. (2017a) indicated that, in the CPM simulations produced by Liu et al. (2017), the frequency of intense summertime MCS is projected to more than triple, and the total MCS precipitation volume is expected to increase by up to 80% in North America by the end-of-century under RCP8.5. Fitzpatrick et al. (2020) reported that the CPM simulations of Africa project a 28% increase in the extreme rain rate of MCSs by the end of the twenty-first century under RCP8.5, which is primarily explained by the projected increases in total column water. Hwang et al. (2023) conducted 4-km CPM simulations spanning 15 years for both current and future periods covering the central U.S.; they found significant changes in the initiation, longevity, and rain rates of warm-season MCSs under the Shared Socioeconomic Pathway 2-8.5 (SSP2-8.5) scenario, with precipitable water (PW) identified as the most crucial variable in understanding future changes. Haberlie et al. (2023) examined the 3.75-km CPM simulations produced by Gensini et al. (2023) and found the proportion of precipitation associated with MCSs significantly increases across the U.S. in both end-of-21st-century climate change scenarios (RCP4.5 and RCP8.5).

Despite these advancements, studies of precipitation and MCSs and the associated climate change impacts using high-resolution CPM regional climate simulations remain limited in many parts of the world, such as South America, especially the Peruvian Central Andes, which is a region characterized by complex terrain and highly susceptible to the impacts of climate change (Schumacher and Rasmussen, 2020). Almazroui et al. (2021) analyzed the ensemble of GCMs from the Coupled Model Intercomparison Project Phase 6 (CMIP6) over South America and found that future precipitation exhibits an increase over the Peruvian Central Andes but a decrease over the Amazon Basin at the middle and end of the twenty-first century, and the changes are consistent across four SSPs: SSP1–2.6, SSP2–4.5, SSP3–7.0 and SSP5–8.5. Hodnebrog et al. (2021) downscaled three GCMs to 50- and 10-km grid spacings covering Peru and found inconsistent precipitation trend projections as the model resolution increased. This resolution dependency suggests that CPM simulations are necessary to enhance the reliability of precipitation and MCS projections in this region, because both 50- and 10-km grid spacing models strongly rely on the highly uncertain cumulus parameterization to produce convective precipitation. Potter et al. (2023) used a bias-corrected 4-km CPM simulation as the historical

baseline and an ensemble of statistically downscaled CMIP5 models to reveal substantial increases in precipitation extremes and intensified meteorological droughts over the two most glacierized regions of Peru by the late twenty-first century under RCP8.5. However, uncertainties may arise from inconsistencies between the historical dynamical downscaling and the future statistical downscaling. Thus, the use of CPM climate simulations is highly desirable to produce more reliable future projections of precipitation and MCS activities in the Peruvian Central Andes region.

The primary objective of this study is to fill the noted gap by producing CPM future projections and examining projected changes in precipitation patterns and MCSs in the Peruvian Central Andes region. This research is crucial for understanding regional hydrological cycles and extreme weather events, such as flash floods, in different climate change scenarios. Our findings will contribute to the growing body of evidence highlighting the benefits and advantages of CPMs in climate projections, especially in regions characterized by complex terrain like the Central Andes.

The remainder of the paper is structured as follows: Section 2 describes the method and the datasets employed. Section 3 presents and discusses the projected changes in precipitation and MCSs. Conclusions and summary remarks are presented in Section 4.

2 | METHOD AND DATA

Both historical and future simulations in this study adopt the same model setup and physics scheme configurations as detailed in Huang et al. (2023a,b). Specifically, the simulations use WRF V4.2.1 (Skamarock et al., 2019) with two one-way nested domains, covering the entire South America with a 15-km horizontal grid spacing, and the Peruvian Central Andes with a 3-km horizontal grid spacing, respectively. The physics schemes employed for both domains include Mellor-Yamada-Nakanishi-Niino (MYNN) level 2.5 planetary boundary layer (PBL) scheme (Nakanishi and Niino, 2009), Thompson microphysics scheme (Thompson et al., 2008), Unified Noah land surface model (Ek et al., 2003), revised MM5 Monin-Obukhov surface layer scheme (Jiménez et al., 2012), and Rapid Radiative Transfer Model for GCMs (RRTMG) longwave and shortwave radiation schemes (Iacono et al., 2008). Tiedtke cumulus scheme (Tiedtke, 1989) and spectral nudging are activated only in the outer domain (Huang et al., 2023b). The choice of the physics parameterization schemes is based on a larger number of sensitivity experiments run over a shorter period (Huang et al., 2023b) and two six-year historical runs (Huang et al., 2023a).

Due to computational resource constraints, two historical simulations were run using two different PBL schemes, spanning the period from 2014 to 2019, with the first year as the spin-up period. Huang et al. (2023a) show that the simulation using the MYNN PBL scheme, as described above, has a better performance in precipitation simulation, and is therefore used as the historical benchmark in this study. We refer to this historical simulation as HIST and its physics configuration is also used for future projection simulations. The initial and boundary conditions of HIST are from the hourly ECMWF Reanalysis v5 (ERA5; Hersbach et al., 2020). An evaluation by Huang et al. (2023a) indicates that HIST can successfully reproduce the main spatiotemporal patterns of precipitation and MCSs in the Peruvian Central Andes region, and thus demonstrates the feasibility of CPM simulations with a limited historical period for projecting potential climate change impacts on precipitation and MCSs within the region.

Two decade-long future simulations were conducted for the period 2070–2080 under two distinct SSP scenarios: SSP2-4.5 and SSP5-8.5, corresponding to the intermediate and very high greenhouse gas emission scenarios in CMIP6, respectively. The initial year (2070) serves as the spin-up period for both simulations. The two future simulations, hereinafter referred to as SSP245 and SSP585, respectively, are driven by a bias-corrected global future climate projection dataset based on the CMIP6 multi-model ensemble (Xu et al., 2021). The bias-corrected global dataset is derived from 18 better CMIP6 models run for the two SSP scenarios together with the ERA5 reanalysis (for bias

correction), which has been shown to have a better representation of the climatological mean, interannual variance, and extreme events than the individual CMIP6 model projections (Xu et al., 2021). This dataset has been used in several recent dynamical downscaling studies in different regions (Chang et al., 2023; Wang et al., 2023; Wu and Zheng, 2023; Yang et al., 2023). To be consistent, time-varying concentrations of greenhouse gases, as employed in the CMIP6 Scenario Model Intercomparison Project (ScenarioMIP) for SSP2-4.5 and SSP5-8.5 scenarios (O'Neill et al., 2016), were adopted in the WRF longwave and shortwave radiation schemes in the corresponding future simulations SSP245 and SSP585.

The annual mean 2-m air temperature differences between SSP245 and HIST are found to be ~2.09°C, ~1.92°C, and ~2.03°C for the mountain, foothill, and Amazon Basin regions, respectively. These corresponding differences between SSP585 and HIST are ~3.45°C, ~3.24°C, and ~3.33°C, respectively.

To examine changes in MCS characteristics, hourly precipitation data from both historical and future simulations are used to identify and track MCSs with an object-tracking method, which employs a precipitation intensity threshold of 5 mm h^{-1} and a minimum precipitation object area of 1000 km^2. For more details on the identification of MCSs, see Huang et al. (2023a).

3 | RESULTS

3.1 | Changes in precipitation

In comparing annual precipitation patterns from the historical simulation (HIST) with future projections (SSP245 and SSP585) (Figs. 1a–c), it is evident that the SSP245 and SSP585 scenarios project a consistent trend: decreased annual precipitation over the western Amazon Basin and increased annual precipitation along the Peruvian west coast in regions below 1-km elevation, as well as in some regions on the east slope of the Andes above 1-km elevation (Figs. 1d, e, g, and h). These changes are generally consistent with the results of GCM projections (Almazroui et al., 2021). Notably, the western Amazon Basin exhibits reductions in annual precipitation of up to 1 mm day^{-1} (as shown in Figs. 1d and e), corresponding to a decrease of less than 20% (Figs. 1g and h) for both SSP245 and SSP585. Contrastingly, along the west coast, particularly in desert areas, the increase in annual precipitation can exceed 200%. Variations in annual precipitation within the four identified precipitation "hotspots" along the east slope of the Andes (highlighted by rectangles) are less uniform and generally not significant, characterized mostly by increased precipitation in areas above 1-km elevation and decreased precipitation below this elevation. The differences in annual precipitation between SSP245 and SSP585 are marginal across most regions (Figs. 1f and i). For a clearer depiction, Fig. 2 presents the area-averaged annual precipitation in six selected regions (indicated in Fig. 1). Similarly, in regions 1–4 along the east slope of the Andes and region 6 on the west slope, differences between HIST and future simulations (SSP245 and SSP585) are not substantial. However, a significant reduction in annual precipitation in SSP245 and SSP585 compared to HIST is observed in region 5, located over the western Amazon Basin (Fig. 2). Interestingly, all six regions exhibit an increase in the standard deviation of annual precipitation in SSP245 and SSP558 relative to HIST (Fig. 2), indicating an enhanced variability in annual precipitation in a warming climate. It is also noteworthy that annual precipitation is predominantly influenced by precipitation during the austral summer. The differences in warm-season precipitation between the HIST and future simulations are similar to those seen in annual precipitation (not shown).

To examine the sub-daily precipitation, Fig. 3 displays the frequency distributions of hourly precipitation across the six regions of interest (as depicted in Fig. 1) for HIST, SSP245, and SSP585. Distinct rightward shifts in precipitation intensity are witnessed when comparing the historical data (HIST) with future projections (SSP245 and SSP585) (Figs. 3a–f). In general, there is a clear trend of increased precipitation intensity at higher percentiles in both future

simulations, indicating a potential for more frequent extreme hourly precipitation events in a warmer climate. This trend is apparent in both humid areas, such as the identified precipitation hotspots along the east slope of the Andes (regions 1–4, Figs. 3a–d) and the western Amazon Basin (region 5, Fig. 3e) as well as in arid zones such as region 6 (Fig. 3f). At the 99.9th percentile, the precipitation intensity is notably higher in future simulations, up to a 12.1% increase in region 4 for SSP245 (Fig. 3d) and up to a 16.9% increase in region 6 for SSP585 (Fig. 3f), compared to HIST. These increases underscore a potential intensification of the most extreme hourly precipitation events under the SSP2-4.5 and SSP5-8.5 scenarios. Moreover, the difference between the two future scenarios becomes more pronounced with the increase of precipitation intensity, especially at the 99.9th percentile. For instance, precipitation at the 99.9th percentile in region 6 exhibits an increase of up to 10.2% when comparing SSP585 to SSP245 (as shown in Fig. 3f). It suggests that the SSP5-8.5 scenario, which assumes the highest radiative forcing, could lead to a significant amplification in the frequency and intensity of extreme hourly precipitation events. Besides, the analysis of the diurnal cycle of precipitation yields no significant changes in the diurnal precipitation phase and the spatial pattern of diurnal precipitation peak time. Additionally, variations in the intensity of diurnal precipitation do not display a consistent trend across the various regions or seasons (not shown). This suggests that while other aspects of precipitation may be affected by climatic changes, the diurnal cycle of precipitation, at least in terms of peak timing and intensity, remains relatively stable. This is not surprising as the forcing mechanisms for precipitation diurnal cycles are not expected to change much with climate warming.

Overall, changes in annual precipitation are location-dependent. Under both the SSP2-4.5 and SSP5-8.5 future scenarios, there is a general decrease in annual precipitation over the western Amazon Basin but an increase along the Peruvian west coast in areas below 1-km elevation and on the east slope of the central Andes above 1 km. Moreover, there is a consistent increase in the frequency of extreme hourly precipitation events across all examined regions including both humid and arid regions under the SSP2-4.5 and particularly under the SSP5-8.5 scenarios compared to HIST. This suggests a consistent trend toward more frequent intense precipitation events in the future, regardless of the typical humidity levels of the regions.

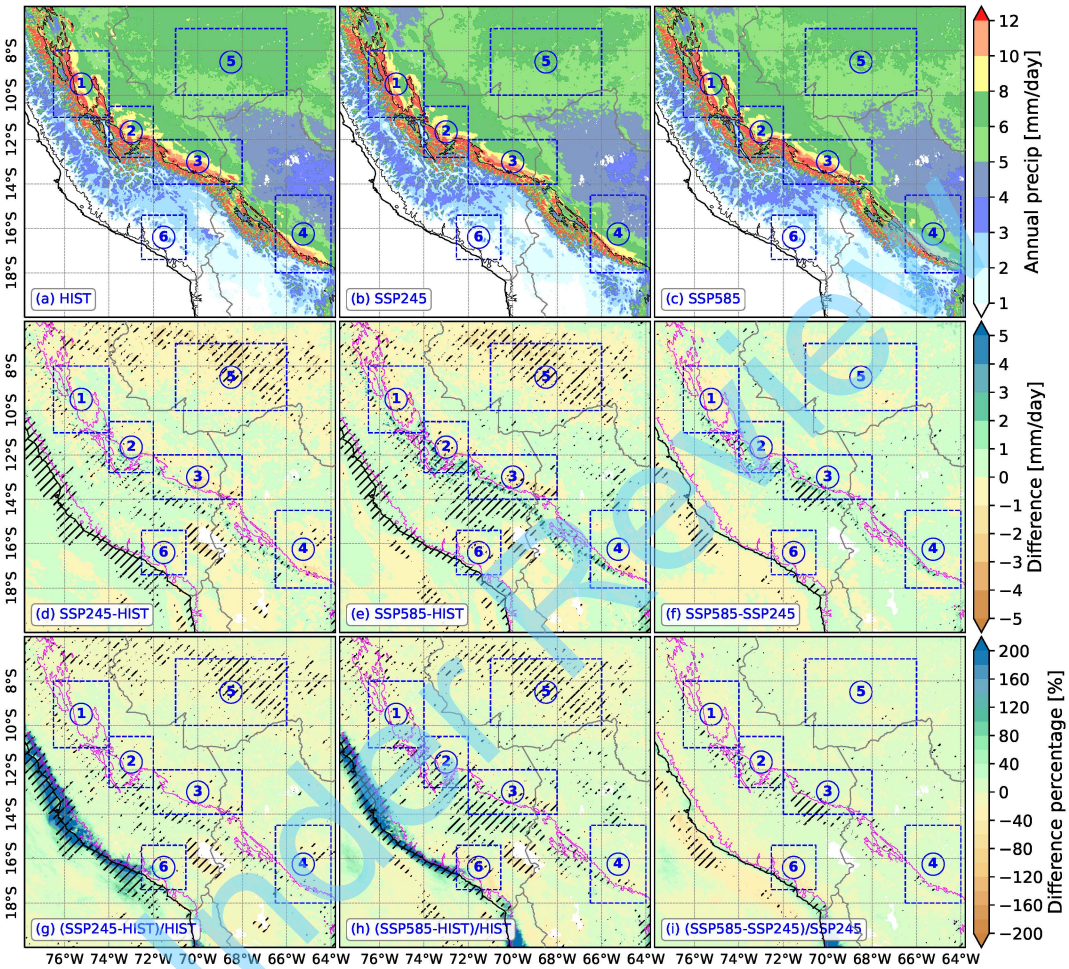

FIGURE 1 Average annual precipitation (mm day^{-1}) in (a) HIST, (b) SSP245, and (c) SSP585. The differences in average annual precipitation (mm day^{-1}) are presented between (d) SSP245 and HIST, (e) SSP585 and HIST, (f) SSP585 and SSP245, and panels (g) to (i) depict their corresponding percentage difference (%). The magenta contour in each panel indicates the terrain elevation of 1 km. Areas marked with a slash pattern in (d)–(i) indicate that the differences are statistically significant at the 0.05 level. The dashed blue rectangles represent the regions used for calculating the area-averaged annual precipitation shown in Fig. 2.

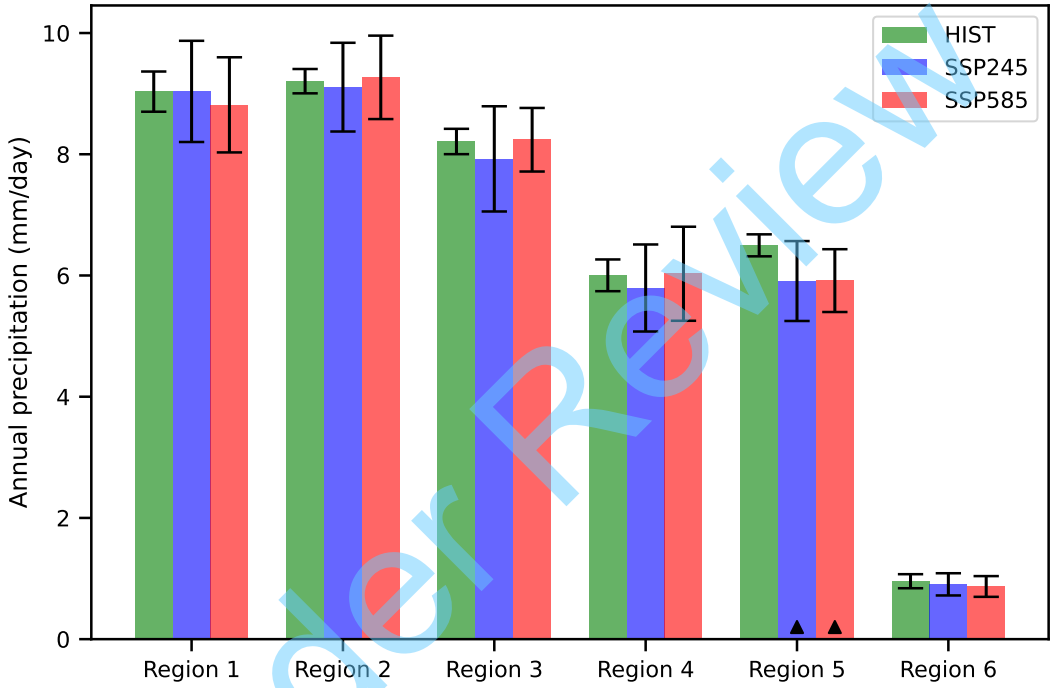

FIGURE 2 Area-averaged annual precipitation (mm day^{-1}) for HIST (green), SSP245 (blue), and SSP585 (red) in the six regions shown in Fig. 1. The error bars represent the range of ± one standard deviation. The black triangles indicate the differences in mean annual precipitation between the historical (HIST) and the future simulations (SSP245 and SSP585) are statistically significant at the 0.05 level.

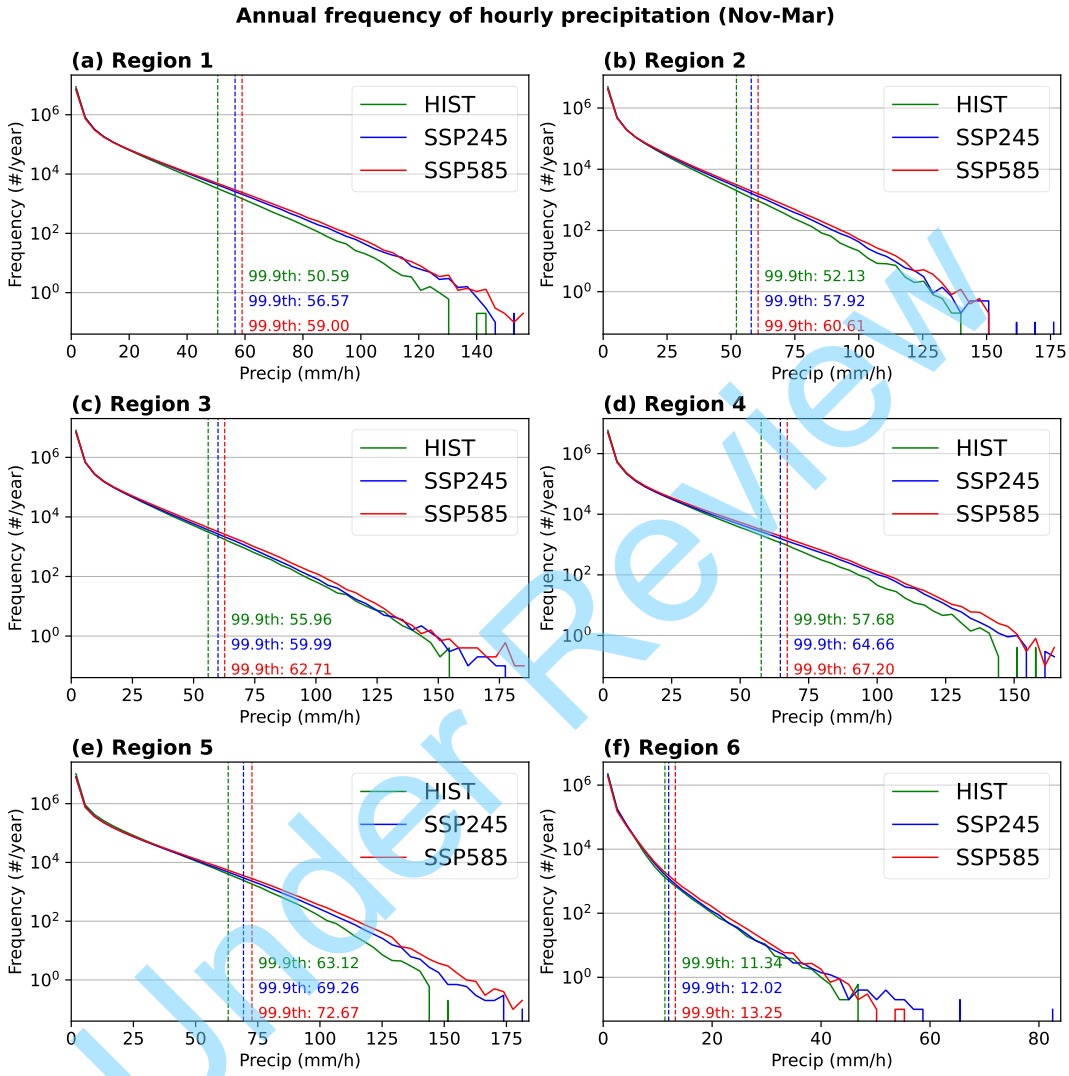

FIGURE 3 Averaged frequency (# year^{-1}) distribution of hourly precipitation (mm h^{-1}) for HIST (green), SSP245 (blue), and SSP585 (red) in the six regions shown in Fig. 1. This analysis considers only data points where hourly precipitation exceeds 0.01 mm h^{-1} during the warm season (November to March). The Kolmogorov-Smirnov test reveals that the differences in distributions between the historical (HIST) and the future simulations (SSP245 and SSP585) are statistically significant at the 0.05 level. The vertical dashed lines mark the 99.9th percentile of precipitation values (in mm h^{-1}).

3.2 | Changes in MCS characteristics

Previous studies have highlighted the significant role of MCSs in contributing to annual precipitation in the Peruvian Central Andes region (Feng et al., 2021; Huang et al., 2023a; Paccini and Stevens, 2023). Additionally, MCSs are frequently associated with heavy precipitation and can result in severe flooding (Schumacher and Rasmussen, 2020). In light of their critical impacts, this section focuses on examining the projected changes in the activities and properties of MCSs in the Peruvian Central Andes region.

In the historical simulation HIST, MCSs contribute over 25% of the annual precipitation and more than 30% at specific locations along the east slope of the Andes and over the western Amazon Basin (Fig. 4a). This contribution is somewhat lower than the values indicated in other studies based on coarser resolution gridded precipitation products, such as the Integrated Multi-satellitE Retrievals for GPM (IMERG, at a grid spacing of 0.1°) (e.g., Feng et al., 2021). This discrepancy can be attributed primarily to two factors: the different MCS definitions adopted in this study compared to others (Feng et al., 2021; Huang et al., 2023a), and the underestimate of MCS size in CPM simulations relative to those identified in gridded precipitation products (Huang et al., 2023a). A significant amount of annual precipitation results from hourly precipitation exceeding 5 mm h^{-1} east of the Andes in CPM simulations, but these events occur in areas smaller than the precipitation area threshold of 1000 km^2 for MCS identification (not shown). Despite these differences in the specific values of MCS contributions to annual precipitation, comparative analysis of future simulations (SSP245 and SSP585) against the historical data (HIST) remains a viable method to assess relative changes in MCS contributions to annual precipitation. In the future simulations (SSP245 and SSP585, Figs. 4b and c), the regions where the contribution of MCS precipitation to annual total precipitation exceeds 25% extends over most areas east of the Andes. Notably, areas with MCS contributions exceeding 30% expand in future simulations, with the highest contributions exceeding 40%, particularly in SSP585. Almost all areas east of the Andes within the study domain exhibit an increase in MCS precipitation contribution, with some areas experiencing increases of over 15% in both SSP245 and SSP585 (Figs. 4d and e). This trend occurs despite a decrease in annual precipitation in some regions, especially over the western Amazon Basin (Figs. 1d and e). Furthermore, the difference in percentage between the future simulations (SSP245 and SSP585) and the historical simulation (HIST) can exceed 200% along the east slope of the Andes (Figs. 4g and h). Although there are no significant differences in annual precipitation between SSP245 and SSP585 (Figs. 1f and i), SSP585 shows a MCS precipitation contribution up to 9% (over 20% in percentage) higher in most areas east of the Andes (Figs. 4f and i).

Figure 5 displays the seasonal distribution of MCS genesis frequency in HIST, SSP245, and SSP585 as well as their differences. In HIST, the occurrence of MCSs is concentrated in specific regions, mainly at the precipitation hotspots along the east slope of the Andes and over the western Amazon Basin, with a higher frequency during the DJF (December-January-February) and MAM (March-April-May) seasons (Figs. 5a1–a4). Compared to HIST, SSP245 and SSP585 exhibit an overall increase in the genesis frequency of MCSs at the MCS genesis hotspots across all seasons, especially in DJF and MAM (Figs. 5b1–e4). The differences in the genesis of MCSs between the future and historical simulations (SSP245 minus HIST and SSP585 minus HIST) can be up to three MCSs per season, especially along the eastern Andes in DJF and MAM (Figs. 5d1–e4). The difference between SSP585 and SSP245 suggests a further increase in MCS genesis frequency under the more extreme SSP5-8.5 scenario compared to SSP2-4.5, predominantly during DJF and MAM (Figs. 5f1–f4). Therefore, the results indicate a projected increase in MCS activity under future climate warming scenarios, suggesting a trend towards more frequent and intense organized storms in a warmer climate. This trend is likely to have a significant impact on regional precipitation patterns and extremes.

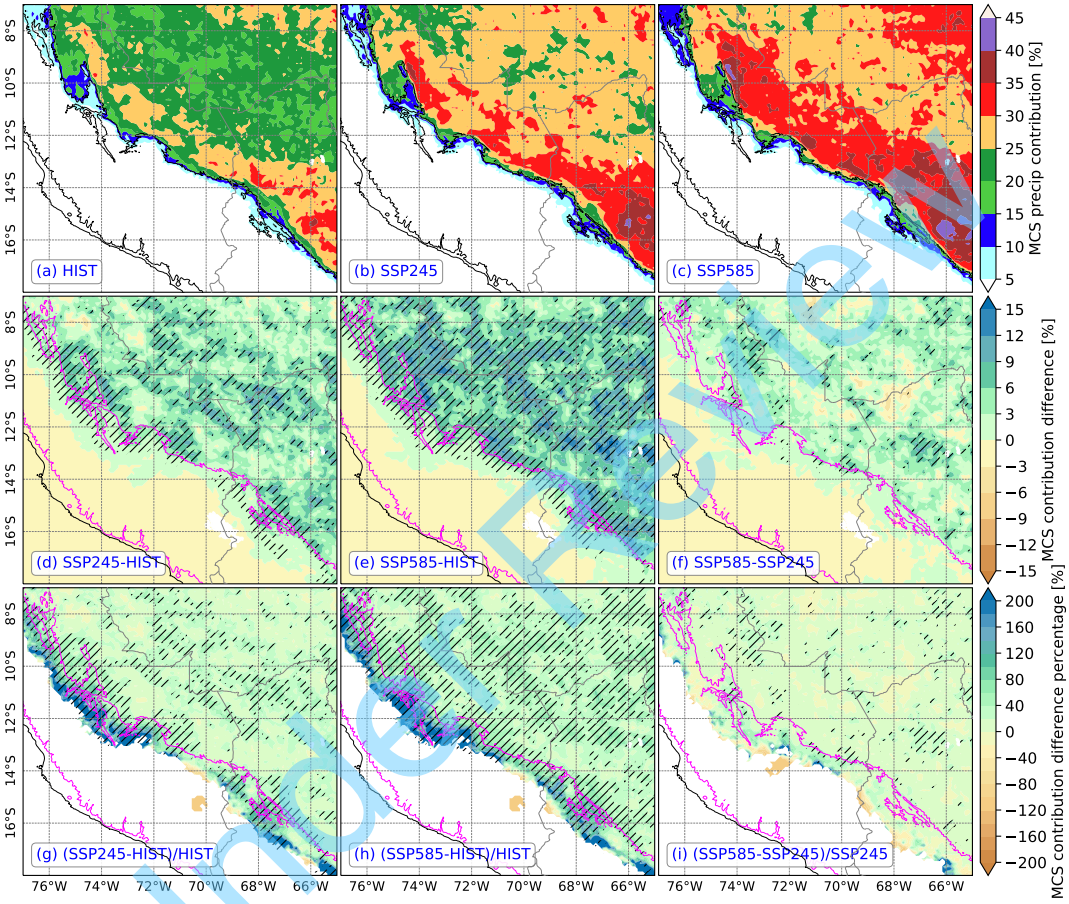

FIGURE 4 Contribution (%) of MCS precipitation to the annual precipitation for (a) HIST, (b) SSP245, (c) SSP585. The differences in contributions are shown between (d) SSP245 and HIST, (e) SSP585 and HIST, and (f) SSP585 and SSP245. Panels (g) to (i) are percentage differences. Areas marked with a slash pattern in (d)–(i) indicate that the differences are statistically significant at the 0.05 level. The magenta contour in each panel indicates the terrain elevation of 1 km.

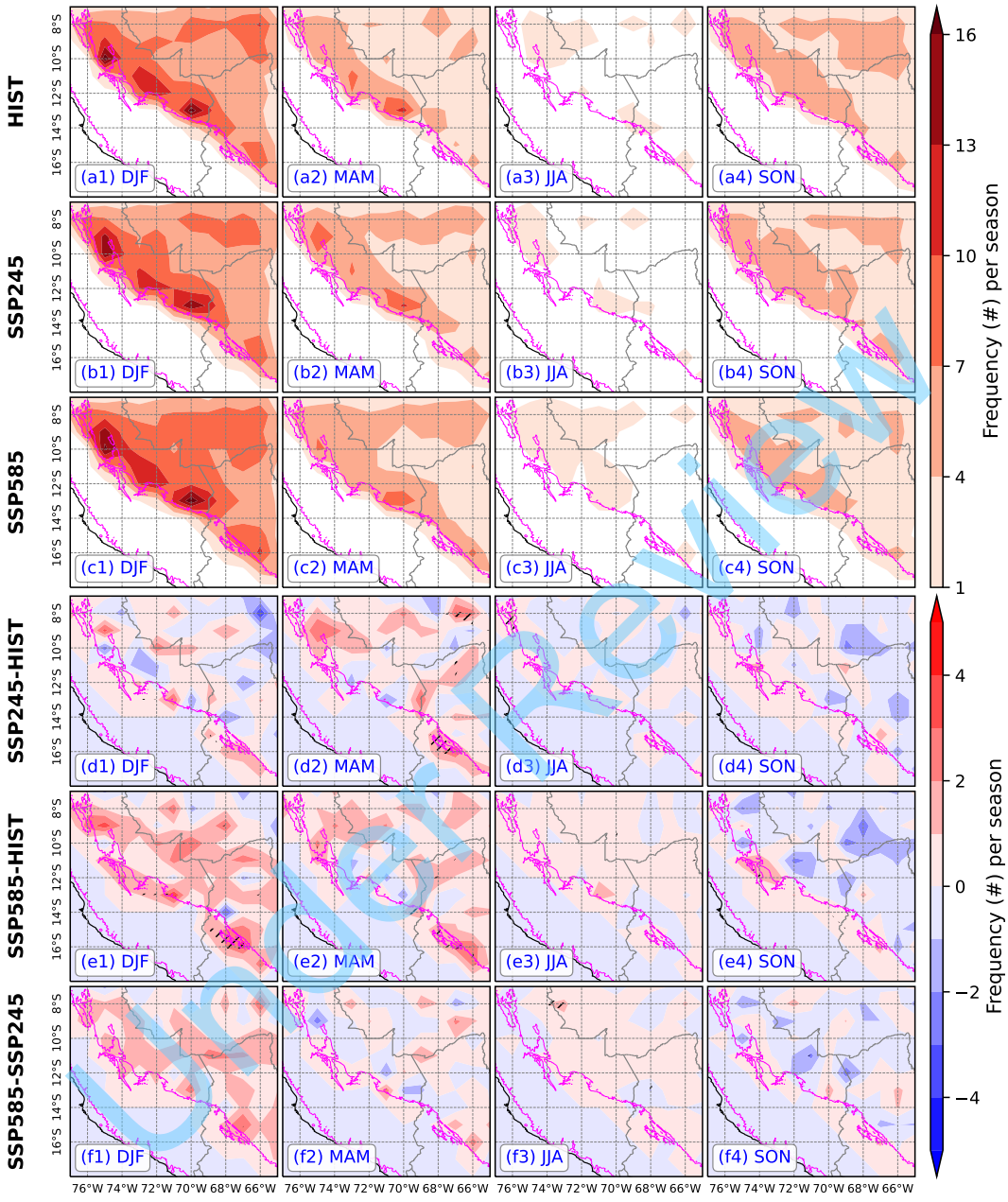

FIGURE 5 Distribution of MCS genesis frequency (counted per bin) in a 1° × 1° latitude/longitude grid in each season for (a1–a4) HIST, (b1–b4) SSP245, and (c1–c4) SSP585. Frequency differences are depicted between (d1–d4) SSP245 and HIST, (e1–e4) SSP585 and HIST, and (f1–f4) SSP585 and SSP245. (a1–f1) Summer: December-January-February (DJF), (a2–f2) Autumn: March-April-May (MAM), (a3–f3) Winter: June-July-August (JJA), and (a4–f4) Spring: September-October-November (SON). Areas marked with a slash pattern in (d1)–(f4) indicate that the differences are statistically significant at the 0.05 level. The magenta contour in each panel indicates the terrain elevation of 1 km.

To further examine the changes in MCS characteristics, violin plots are employed to illustrate the distribution of key MCS attributes for the historical and future simulations, including hourly mean precipitation, peak hourly precipitation, size, duration, hourly precipitation volume (hourly mean precipitation × MCS size), and movement speed (Fig. 6). For the MCS hourly mean precipitation, HIST shows a median value around 16.2 mm h^{-1}, while SSP245 and SSP585 indicate a slight increase to ~16.8 and ~17.4 mm h^{-1}, respectively (Fig. 6a), corresponding to an increase of ~3.7% and ~7.4%, respectively. The extreme values of hourly mean precipitation, here represented by 1.5 times the interquartile range (IQR), increase by ~5.3% in SSP245 (27.8 mm h^{-1}) and ~9.5% in SSP585 (28.9 mm h^{-1}) compared to HIST (26.4 mm h^{-1}) (Fig. 6a). Peak hourly precipitation (Fig. 6b) shows a more notable increase in the median and extreme values across the simulations. The median value of peak hourly precipitation increases from 48.2 mm h^{-1} in HIST to 50.8 mm h^{-1} in SSP245 (an increase of ~5.4%) and 53.0 mm h^{-1} in SSP585 (an increase of ~10.0%). Moreover, the extreme value of peak hourly precipitation rises from 93.4 mm h^{-1} in HIST to 100.4 mm h^{-1} in SSP245 with an increase of ~7.5% and 104.8 mm h^{-1} in SSP585 with an increase of ~12.2% (Fig. 6b). The size of MCSs follows a similar upward trend, with median and extreme values increasing by ~4.8% and ~10.5% in SSP245, and by ~5.1% and ~11.5% in SSP585 respectively, compared to HIST (Fig. 6c), suggesting MCS enlargement in future warming scenarios. Furthermore, the MCS hourly precipitation volume (Fig. 6e), calculated as the product of hourly mean precipitation and MCS size, shows an increase in extreme values from 0.18 km^3 h^{-1} in HIST to 0.21 and 0.22 km^3 h^{-1} in SSP245 and SSP585, increasing by ~16.7% and ~22.2%, respectively. The MCS duration shows less variability across simulations with a median of 3 hours and the differences in their distributions are not significant between the historical simulation and the future simulations (Fig. 6d). However, the extreme value in the MCS duration increases from 12 hours in HIST to 14.5 hours in SSP245 and SSP585, a rise of ~20.8% (Fig. 6d). It suggests that extremes in all examined MCS characteristics are projected to intensify under future warming conditions. Meanwhile, the MCS movement speed shows a slight increase in median and extreme values in SSP245 and SSP585 compared to HIST (Fig. 6f). Taken together, compared to the historical simulation, the future simulations generally project an intensification of MCSs in terms of precipitation intensity and size, which could lead to amplified impacts on precipitation, flooding, and other related hazards.

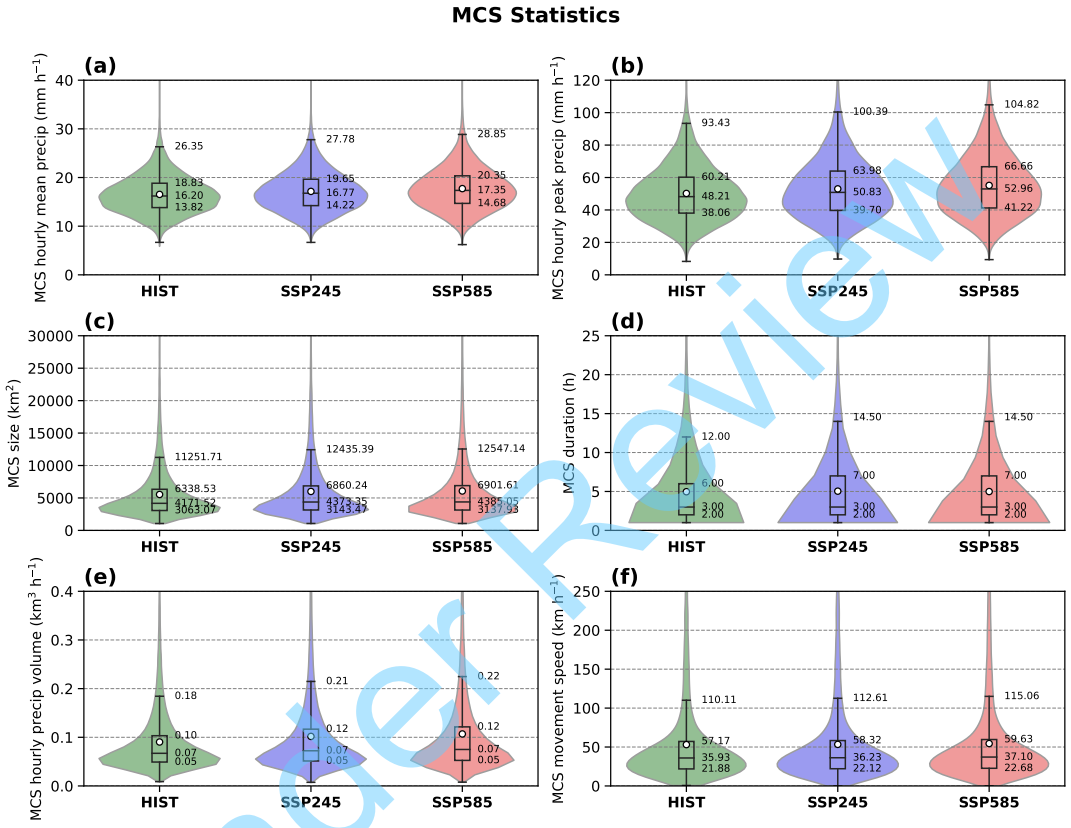

FIGURE 6 Violin plots illustrate the distribution of various MCS properties, including (a) hourly mean precipitation, (b) hourly peak precipitation, (c) size, (d) duration, (e) hourly precipitation volume, and (f) movement speed for the HIST, SSP245, and SSP585. Within the accompanying box-and-whisker plots, the white circles denote the average values of the samples. Additionally, the 25th, 50th, and 75th percentiles, along with 1.5 times the interquartile range (IQR), are delineated adjacent to these plots. The distributions of HIST and the future simulations (SSP245 and SSP585) show significant differences at the 0.05 level, except for MCS duration in the comparisons of HIST with both SSP245 and SSP585, and for movement speed in the comparison between HIST and SSP245.

3.3 | Changes in dynamic and thermodynamic conditions

The following section delves into the dynamic and thermodynamic fields to gain an understanding of the mechanisms driving the changes in precipitation patterns and MCS characteristics. Given that precipitation in the study region predominantly occurs during summer (DJF), the averaged dynamic and thermodynamic fields in DJF are examined here.

The average wind vectors at 850 hPa during DJF at the four times of the day show a prevailing wind direction parallel to the Andes on the east of Andes, persisting throughout the day (Figs. 7a1–a4). This pattern is predominantly shaped by the high, steep Andes and the South American low-level jet (SALLJ) (Marengo et al., 2002, 2004; Vera et al., 2006). Wind speeds display obvious diurnal variations in both the slope and basin regions, as distinctly illustrated in the vertical profiles of diurnal wind speeds (Fig. 8). Such variations are largely influenced by changes in the boundary layer mixing. The wind speed decreases during the daytime due to mixing and accelerates during the night as the surface frictional effect on the boundary layer flow fades (Fig. 8). At 850 hPa, the spatial patterns of the wind field are very similar between the historical and future simulations (not shown), with the primary distinction being an increase in wind speeds, particularly in the corridor stretching from the eastern Andean foothills to the western Amazon Basin in the future simulations (Figs. 7b1–b4 and c1–c4). The average vertical wind profiles (Figs. 8a1–c1) in the slope region show an increase in maximum wind speeds from slightly above 3.0 m s^{-1} in HIST to over 4.0 m s^{-1} in SSP245 and exceeding 4.5 m s^{-1} in SSP585. A similar increase in wind speed is displayed in the basin region, from HIST to SSP245 and SSP585 (Figs. 8a2–c2), while the wind speeds in the basin region are consistently higher than those in the slope region (Fig. 8). A notable characteristic of SSP245 and SSP585 is the elevation increase of the maximum wind speed cores relative to HIST in both the slope and basin regions (Fig. 8). This behavior could be due to deeper mixed boundary layers under warming conditions, but is equally likely related to changes in large-scale atmospheric circulations. The small-domain CPM simulations produced in this study do not provide sufficient data to thoroughly investigate variations in large-scale circulations. It is worth investigating in the future, possibly with the help of GCM simulations.

Understanding the divergence field is crucial for comprehending the relationship between precipitation and dynamic fields. Huang et al. (2023a) demonstrated that precipitation and the genesis of MCSs along the east slope of the Andes are predominantly influenced by dynamic factors, particularly the low-level jet and terrain-induced uplift. In HIST, the patterns of divergence at 10 and 16 LST and convergence at 22 and 04 LST along the east slope of the Andes (Figs. 7a1–a4) align with the diurnal precipitation variation in this region. Although the low-level jet shows an intensification in SSP245 and SSP585 (Figs. 8a1–c1), the enhancement in convergence along the Andean east slope is not consistently shown (Figs. 7b1–c3). This inconsistency is dependent on wind direction and the influence of terrain notches. Therefore, both increases and decreases in annual precipitation exist along the east slope of the Andes (Fig. 1), indicating more complex relationships between dynamic processes and precipitation patterns in mountainous regions. For the western Amazon Basin region, although Huang et al. (2023a) indicated that the precipitation and MCS activity in this region are primarily governed by thermodynamic factors, dynamic convergence remains an essential factor for convection initiation and MCS development. From the differences in divergence fields between the future simulations and the historical simulation (Figs. 7b1–b4 and c1–c4), positive values (red areas) dominate the western Amazon Basin region despite the strengthening of low-level jets, suggesting that convergence weakens in this region in SSP245 and SSP585 compared to HIST. This is consistent with the decrease in annual precipitation over the western Amazon Basin in both future simulations (Fig. 1), underscoring the significant role of dynamic convergence alongside thermodynamic factors in influencing regional precipitation patterns. Moreover, in the comparison between SSP585 and SSP245, there is a notable escalation in the intensity of low-level jets under the more extreme

SSP5-8.5 scenario (Fig. 8). However, this intensification does not translate to stronger convergence at 850 hPa over the western Amazon Basin (Figs. 7d1–d4). This lack of increased convergence aligns with the minimal differences in annual precipitation between SSP585 and SSP245 (Fig. 1).

Overall, while the intensified low-level wind speeds in future warming scenarios are expected to bring more moisture from the tropics to the Peruvian Central Andes region, and a warming climate holds more precipitable water especially east of the Andes (not shown), it is primarily the dynamic divergence that plays a pivotal role in the changes in annual precipitation.

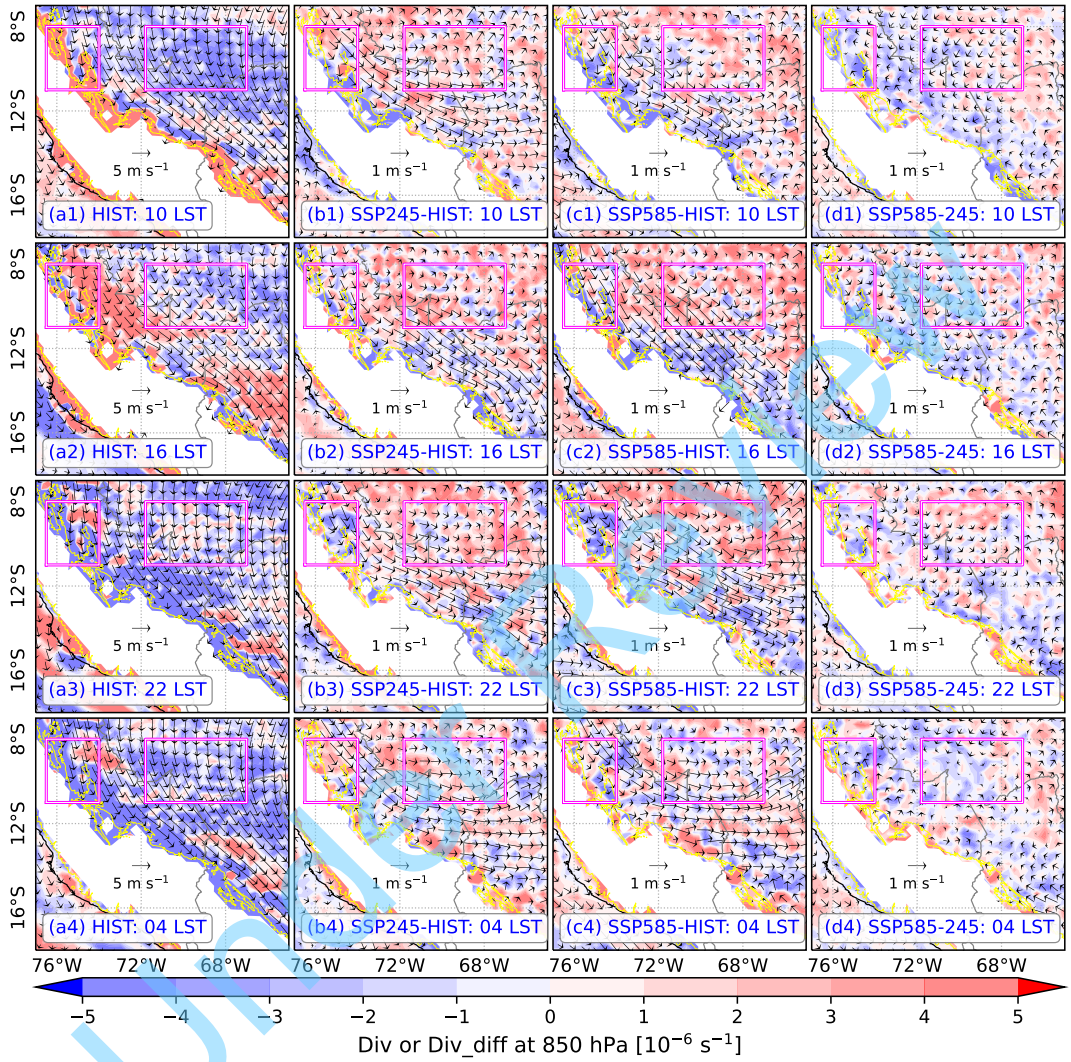

FIGURE 7 Horizontal wind vectors (m s^{-1}) and divergence (shaded, 10^{-6} s^{-1}) at 850 hPa averaged over DJF for (a1–a4) HIST, (b1–b4) differences between SSP245 and HIST, (c1–c4) differences between SSP585 and HIST, and (d1–d4) differences between SSP585 and SSP245 at (a1–d1) 10, (a2–d2) 16, (a3–d3) 22, and (a4–d4) 04 Local Standard Time (LST = UTC − 5 h, corresponding to a longitude of 75°W), respectively. The yellow contour in each panel indicates the terrain elevation of 1 km. The magenta rectangles represent the regions used for area-averaged calculations in Figs. 8 and 9.

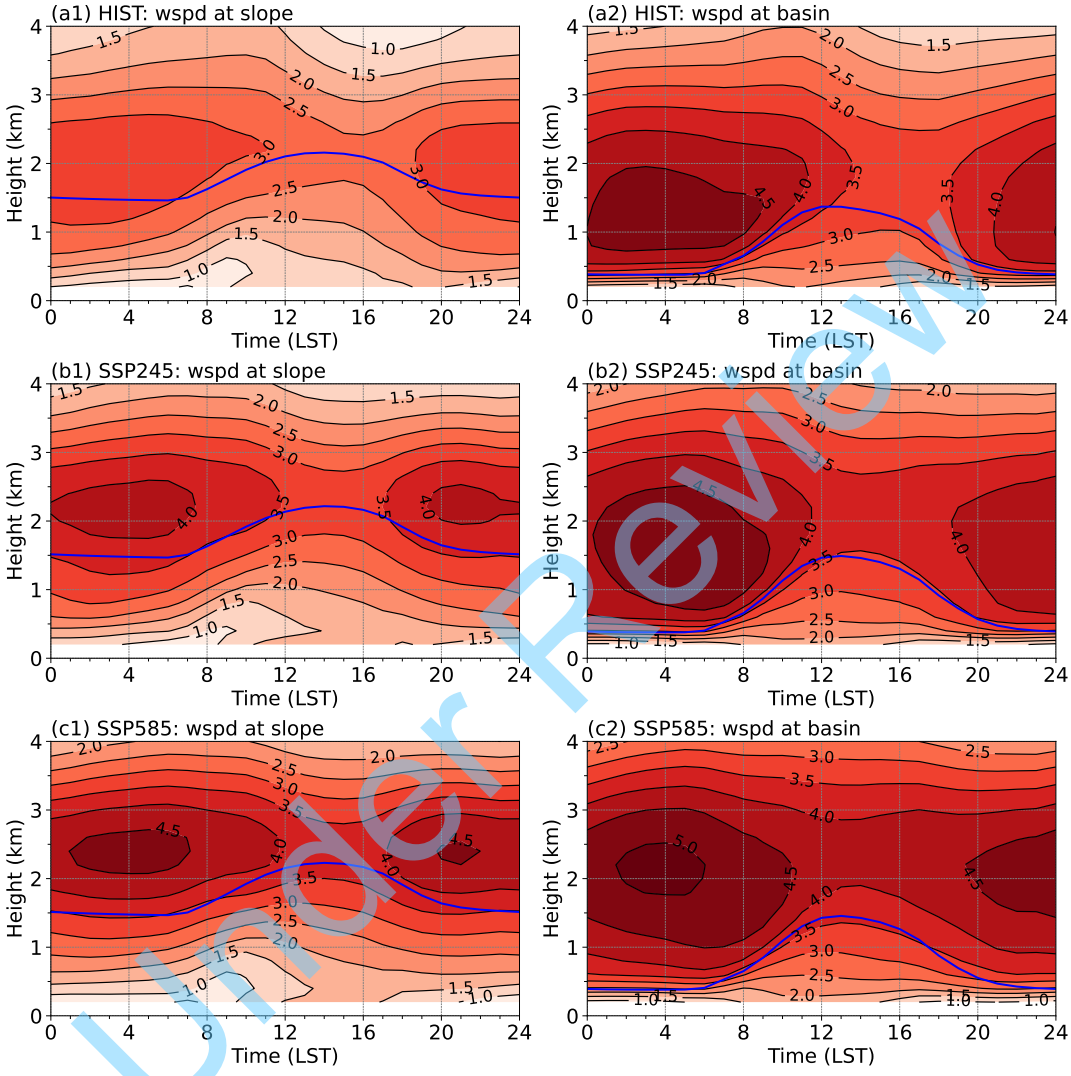

FIGURE 8 Height-time plots depict the area-averaged horizontal wind speeds (m s^{-1}) at MCS genesis hotspots: (a1–c1) along the eastern slope of the Andes and (a2–c2) over the western Amazon Basin (as indicated by the blue rectangles in Fig. 5) in (a1 and a2) HIST, (b1 and b2) SSP245, and (c1 and c2) SSP585. The blue curves represent the boundary layer height (km) above the mean sea level. The x-axis represents the Local Standard Time (LST = UTC − 5 h), corresponding to a longitude of 75°W.

Large-scale dynamic divergence effectively accounts for the overall trends in annual precipitation, while it cannot explain the increased frequency of intense hourly precipitation and the heavy precipitation-producing MCSs in future simulations. This suggests that thermodynamic factors likely exert a more significant influence on the extremes of hourly precipitation. To gain a deeper insight into these influencing factors, the diurnal cycle of key thermodynamic variables is examined. This includes the CAPE, CIN, and PW in both the slope and basin regions (Fig. 9). Analyzing these quantities provides a further understanding of the mechanisms driving the changes in precipitation intensity and frequency in future climate scenarios.

In the slope region, CAPE shows a pronounced diurnal cycle, increasing sharply from 07 LST to around 13 LST, and then decreasing rapidly from 17 LST to the early morning of 06 LST (Figs. 9a1 and a2). This diurnal pattern aligns with the solar radiative heating, the nocturnal intensification of low-level jets (Figs. 8a1–c1), and the diurnal precipitation cycle. There is a significant increase in CAPE at the corresponding LSTs from HIST to the future simulations, with SSP585 showing the most substantial increases (Figs. 9a1 and a2). On average, CAPE increases by ~14.6% in SSP245 and by ~28.4% in SSP585, relative to HIST. The rising CAPE suggests a more unstable atmosphere in a warming climate, which is more conducive to the development of intense convection. Compared to HIST, PW also shows an average increase of ~12.7% for SSP245 and ~21.3% for SSP585 (Fig. 9a2), suggesting an enhanced moisture supply capable of fueling more intense precipitation events. However, a slight increase in CIN is also noted in the future simulations (Fig. 9a1), implying a strengthened energy barrier for convection initiation, which is consistent with the decrease in weak hourly precipitation events (Fig. 3) as well as more stronger convection once initiated.

In the western Amazon Basin (Figs. 9b1 and b2), CAPE begins to increase at 07 LST in response to solar heating, peaks swiftly at 11 LST, and then diminishes, presumably because of convective stabilization, corresponding to the typical pattern of afternoon precipitation development in this region (Huang et al., 2023a). Increases in CAPE from HIST to SSP245 and SSP585 in the basin region are greater in absolute magnitude but of similar percentages to those in the slope region, averaging about 17.8% and 27.5%, respectively (Fig. 9b1). Meanwhile, PW has an increase of ~11.1% in SSP245 and ~19.4% in SSP585 compared to HIST (Fig. 9b2). A similar increase is also found in CIN in the future simulations compared to HIST (Fig. 9b1), implying an enhanced suppression of convective initiation in a warming climate.

Overall, these apparent changes in thermodynamic conditions, characterized by increased CAPE, PW, and CIN, foster an environment conducive to more intense convective precipitation, the formation and intensification of heavy precipitation-producing MCSs, and the suppression of weak precipitation in future warming scenarios. This trend is consistent with the findings in North America (Rasmussen et al., 2020), which report a similar shift in convection population due to increased CAPE and CIN in a warming climate. Such an environmental thermodynamic condition change indicates a tendency to suppress weak convective activity, while concurrently creating a high-CAPE environment for more intense convection. These results emphasize the complex synergy of dynamic and thermodynamic forces in shaping future precipitation patterns, highlighting the vital importance of high-resolution CPM climate modeling for projecting regional hydroclimatic impacts.

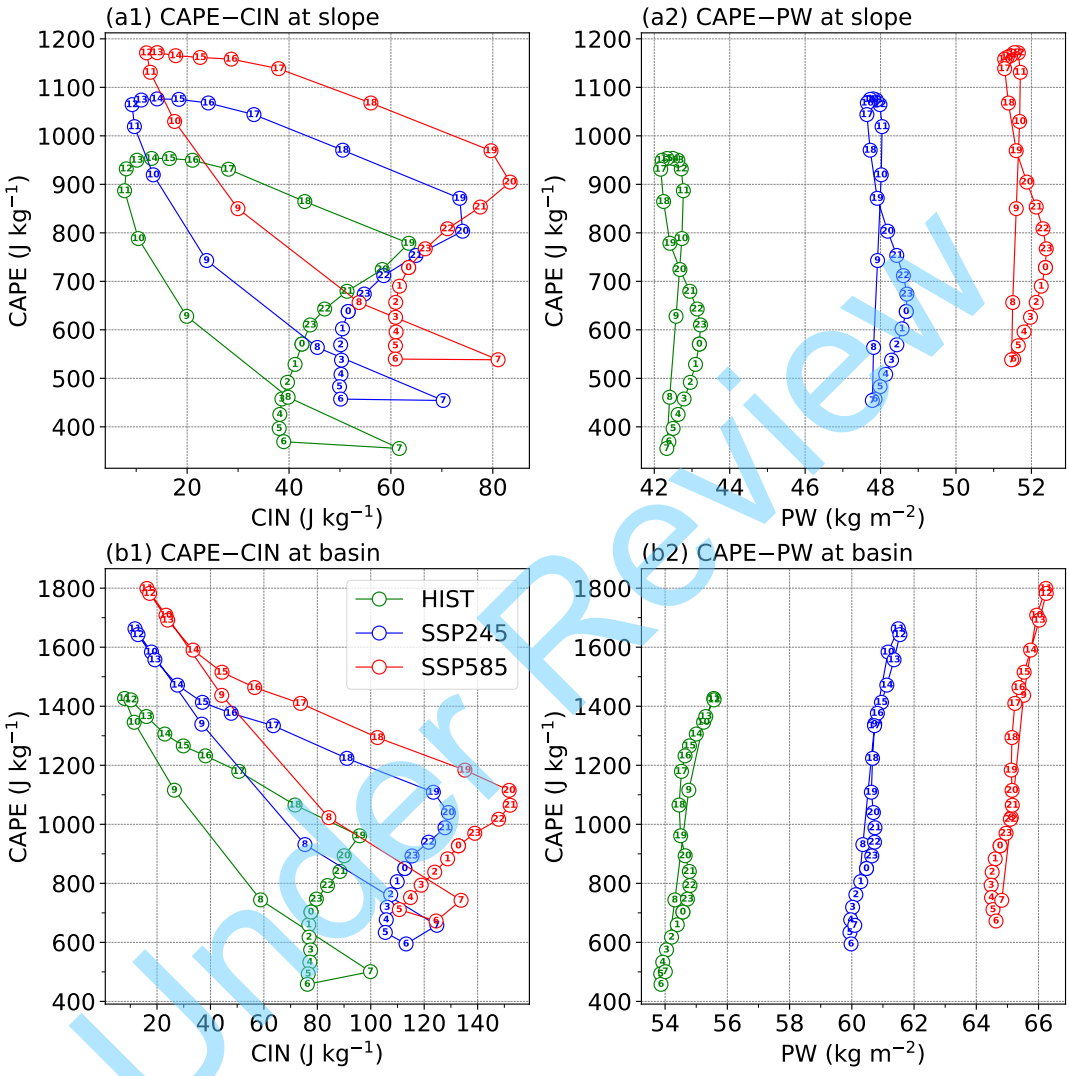

FIGURE 9 Diurnal cycle of (a1 and b1) Convective Available Potential Energy (CAPE, in J kg^{-1}) as a function of Convective Inhibition (CIN, in J kg^{-1}) and (a2 and b2) CAPE as a function of precipitable water (PW, in kg m^{-2}) at MCS genesis hotspots (a1 and b1) along the eastern slope of the Andes and (b1 and b2) over the western Amazon Basin (as indicated by the blue rectangles in Fig. 5). The numbers within the circles represent the Local Standard Time (LST = UTC − 5 h), corresponding to a longitude of 75°W.

4 | SUMMARY

To explore the potential impacts of climate change on precipitation and MCS characteristics in the Peruvian Central Andes region, this study conducts two decade-long future regional climate simulations at a convection-permitting grid spacing, where the WRF model is driven by a bias-corrected global dataset derived from CMIP6 multi-model ensemble under the Shared Socioeconomic Pathways scenarios SSP2-4.5 and SSP5-8.5 corresponding to intermediate greenhouse gas emission and very high greenhouse gas emission scenarios. The simulations cover 11 years from 2070 through 2080 and adopt two nested domains with grid spacings of 15 km and 3 km, covering the entire South America and the Peruvian Central Andes, respectively. The future simulations are compared to a historical simulation over a recent 6-year period, which is driven by ERA5 reanalysis data as described in Huang et al. (2023a). Employing the same model configurations across the historical and future simulations facilitates a direct comparison, enabling a detailed analysis of climate change's potential effects on precipitation and MCSs in the Peruvian Central Andes. The key findings are outlined as follows.

(1) Changes in annual precipitation are geographic location-dependent, while there is a consistent increase in the frequency of intense hourly precipitation across all examined regions including both humid and arid areas in a warming climate. There is a general decrease in annual precipitation over the western Amazon Basin, while an increase exists along the west coast below 1-km elevation and on the east slope of the Andes above 1 km, under both SSP2-4.5 and SSP5-8.5 emission scenarios in comparison to the current climate. Annual precipitation differences between the two future scenarios are marginal across most regions. However, hourly precipitation contrasts become more pronounced, with precipitation intensity increasing by up to 10.2% at the 99.9th percentile under the SSP5-8.5 scenario compared to the SSP2-4.5 scenario.

(2) The future climate simulations under warming scenarios indicate a general increase in various aspects of MCS characteristics on the east of the Andes, including a higher frequency of MCS genesis, an enhancement in MCS precipitation intensity by up to ~10%, and an enlargement in MCS size that can exceed 10%, marking a significant shift from the historical simulation patterns.

(3) In future warming scenarios, synoptic-scale low-level jets are projected to strengthen, while variations in the low-level divergence field dominate the changes in annual precipitation, especially in that the weakened convergence over the western Amazon Basin reduces the annual precipitation there. The thermodynamic conditions in future warming scenarios are characterized by increased CAPE, PW, and CIN. Such changes shift the convection population, by suppressing weak convection while fostering a more unstable and moisture-rich atmosphere conducive to more intense convection and the formation and intensification of heavy precipitation-producing MCSs.

In summary, this study reveals a marked trend in precipitation and MCS activities in the Peruvian Central Andes region under a warming climate: an increase in the frequency of intense hourly precipitation and organized convective storms, coupled with a reduction in weak convective precipitation events. This shift indicates a heightened risk of flash flooding and landslides in this region in the future. The impacts of climate change in this study are shown to be a result of the complex synergy of dynamic and thermodynamic processes as well as interactions with terrain. This complexity underscores the necessity for high-resolution climate modeling to accurately represent regional climate dynamics and local geographical features. The findings not only highlight the value of convection-permitting climate simulations in understanding the hydroclimatic impacts of climate change and projecting future severe weather hazards, particularly in regions with complex terrain such as the Peruvian Central Andes, but also provide critical inputs for developing tailored climate mitigation and adaptation strategies in this region. It should be noted that constraints in computing resources have limited the simulation periods and the range of future climate scenarios in this study, thereby more long-term CPM simulations, such as the 22-year 4-km climate simulations over South America conducted by the South

America Affinity Group (SAAG) (Liu et al., 2022; Dominguez et al., 2024) and the inclusion of a broader range of climate change scenarios are needed to confirm and strengthen the findings in this study. Ensembles of simulations using different model configurations are also desirable to allow for the assessment of model and projection uncertainties.

acknowledgements

This project was primarily supported by grant No. 20163646499 from the Universidad Nacional de San Agustín de Arequipa (UNSA) of Peru through the IREES/LASI Global Change and Human Health Institute. Supplementary funding was provided by the Weathernews Chair funds. Yongjie Huang is partially supported by the DOE ASR project (DE-SC0024317). The authors acknowledge the Texas Advanced Computing Center (TACC) at the University of Texas at Austin (`http://www.tacc.utexas.edu`) for providing HPC resources through XSEDE allocation TG-ATM160014 that are used for the simulations. The authors also acknowledge high-performance computing support from Cheyenne (`https://doi.org/10.5065/D6RX99HX`) provided by NCAR's Computational and Information Systems Laboratory. NCAR is sponsored by the National Science Foundation. Some data processing was performed at the University of Oklahoma (OU) Supercomputing Center for Education and Research (OSCER).

conflict of interest

All co-authors have declared that they do not have any competing interests.

DATA AVAILABILITY STATEMENT

The Bias-corrected CMIP6 global dataset for dynamical downscaling is available at `https://doi.org/10.11922/sciencedb.00487` (last access: 15 December 2021). The model outputs are too large to be publicly archived. Please contact the corresponding author for more information.

references

Almazroui, M., Ashfaq, M., Islam, M. N., Rashid, I. U., Kamil, S., Abid, M. A., O'Brien, E., Ismail, M., Reboita, M. S., Sörensson, A. A. et al. (2021) Assessment of cmip6 performance and projected temperature and precipitation changes over south america. *Earth Systems and Environment*, **5**, 155–183.

Anselmo, E. M., Machado, L. A., Schumacher, C. and Kiladis, G. N. (2021) Amazonian mesoscale convective systems: Life cycle and propagation characteristics. *International Journal of Climatology*, **41**, 3968–3981.

Ascott, M., Christelis, V., Lapworth, D., Macdonald, D., Tindimugaya, C., Iragena, A., Finney, D., Fitzpatrick, R., Marsham, J. and Rowell, D. (2023) On the application of rainfall projections from a convection-permitting climate model to lumped catchment models. *Journal of Hydrology*, **617**, 129097.

Ban, N., Schmidli, J. and Schär, C. (2015) Heavy precipitation in a changing climate: Does short-term summer precipitation increase faster? *Geophysical Research Letters*, **42**, 1165–1172.

Berthou, S., Kendon, E., Rowell, D., Roberts, M., Tucker, S. and Stratton, R. (2019) Larger future intensification of rainfall in the west african sahel in a convection-permitting model. *Geophysical Research Letters*, **46**, 13299–13307.

Berthou, S., Kendon, E. J., Chan, S. C., Ban, N., Leutwyler, D., Schär, C. and Fosser, G. (2020) Pan-european climate at convection-permitting scale: a model intercomparison study. *Climate Dynamics*, **55**, 35–59.

Chan, S. C., Kendon, E. J., Berthou, S., Fosser, G., Lewis, E. and Fowler, H. J. (2020) Europe-wide precipitation projections at convection permitting scale with the unified model. *Climate Dynamics*, **55**, 409–428.

Chang, R., Yan, Y., Wu, J., Wang, Y. and Gao, X. (2023) Projected pv plants in china's gobi deserts would result in lower evaporation and wind. *Solar Energy*, **256**, 140–150.

Chapman, S., Birch, C. E., Galdos, M. V., Pope, E., Davie, J., Bradshaw, C., Eze, S. and Marsham, J. H. (2021) Assessing the impact of climate change on soil erosion in east africa using a convection-permitting climate model. *Environmental Research Letters*, **16**, 084006.

Chen, Y., Paschalis, A., Kendon, E., Kim, D. and Onof, C. (2021) Changing spatial structure of summer heavy rainfall, using convection-permitting ensemble. *Geophysical Research Letters*, **48**, e2020GL090903.

Dominguez, F., Rasmussen, R., Liu, C., Ikeda, K., Prein, A., Varble, A., Arias, P. A., Bacmeister, J., Bettolli, M. L., Callaghan, P. et al. (2024) Advancing south american water and climate science through multi-decadal convection-permitting modeling. *Bulletin of the American Meteorological Society*, **105**, E32–E44.

Ek, M., Mitchell, K., Lin, Y., Rogers, E., Grunmann, P., Koren, V., Gayno, G. and Tarpley, J. (2003) Implementation of noah land surface model advances in the national centers for environmental prediction operational mesoscale eta model. *Journal of Geophysical Research: Atmospheres*, **108**.

Feng, Z., Leung, L. R., Liu, N., Wang, J., Houze Jr, R. A., Li, J., Hardin, J. C., Chen, D. and Guo, J. (2021) A global high-resolution mesoscale convective system database using satellite-derived cloud tops, surface precipitation, and tracking. *Journal of Geophysical Research: Atmospheres*, **126**, e2020JD034202.

Fitzpatrick, R. G., Parker, D. J., Marsham, J. H., Rowell, D. P., Guichard, F. M., Taylor, C. M., Cook, K. H., Vizy, E. K., Jackson, L. S., Finney, D. et al. (2020) What drives the intensification of mesoscale convective systems over the west african sahel under climate change? *Journal of Climate*, **33**, 3151–3172.

Fosser, G., Kendon, E. J., Stephenson, D. and Tucker, S. (2020) Convection-permitting models offer promise of more certain extreme rainfall projections. *Geophysical Research Letters*, **47**, e2020GL088151.

Fosser, G., Khodayar, S. and Berg, P. (2015) Benefit of convection permitting climate model simulations in the representation of convective precipitation. *Climate Dynamics*, **44**, 45–60.

Fumière, Q., Déqué, M., Nuissier, O., Somot, S., Alias, A., Caillaud, C., Laurantin, O. and Seity, Y. (2020) Extreme rainfall in mediterranean france during the fall: added value of the cnrm-arome convection-permitting regional climate model. *Climate Dynamics*, **55**, 77–91.

Gao, Y., Leung, L. R., Zhao, C. and Hagos, S. (2017) Sensitivity of us summer precipitation to model resolution and convective parameterizations across gray zone resolutions. *Journal of Geophysical Research: Atmospheres*, **122**, 2714–2733.

Gensini, V. A., Haberlie, A. M. and Ashley, W. S. (2023) Convection-permitting simulations of historical and possible future climate over the contiguous united states. *Climate Dynamics*, **60**, 109–126.

Giorgi, F. (2019) Thirty years of regional climate modeling: where are we and where are we going next? *Journal of Geophysical Research: Atmospheres*, **124**, 5696–5723.

Guo, Z., Fang, J., Sun, X., Tang, J., Yang, Y. and Tang, J. (2020) Decadal long convection-permitting regional climate simulations over eastern china: evaluation of diurnal cycle of precipitation. *Climate Dynamics*, **54**, 1329–1349.

Haberlie, A. M., Ashley, W. S., Gensini, V. A. and Michaelis, A. C. (2023) The ratio of mesoscale convective system precipitation to total precipitation increases in future climate change scenarios. *npj Climate and Atmospheric Science*, **6**, 150.

Halladay, K., Kahana, R., Johnson, B., Still, C., Fosser, G. and Alves, L. (2023) Convection-permitting climate simulations for south america with the met office unified model. *Climate Dynamics*, 1–23.

Hersbach, H., Bell, B., Berrisford, P., Hirahara, S., Horányi, A., Muñoz-Sabater, J., Nicolas, J., Peubey, C., Radu, R., Schepers, D. et al. (2020) The era5 global reanalysis. *Quarterly Journal of the Royal Meteorological Society*, **146**, 1999–2049.

Hodnebrog, Ø., Steensen, B., Marelle, L., Alterskjaer, K., Dalsøren, S. and Myhre, G. (2021) Understanding model diversity in future precipitation projections for south america. *Climate Dynamics*, 1–19.

Hu, H., Leung, L. R. and Feng, Z. (2021) Early warm-season mesoscale convective systems dominate soil moisture–precipitation feedback for summer rainfall in central united states. *Proceedings of the National Academy of Sciences*, **118**, e2105260118.

Huang, Y., Xue, M., Hu, X.-M., Martin, E., Novoa, H. M., McPherson, R. A., Liu, C., Ikeda, K., Rasmussen, R., Prein, A. F., Perez, A., Morales, I. Y., Ticona, J. L. and Flores, A. J. (2023a) Characteristics of precipitation and mesoscale convective systems over the peruvian central andes in multi 5-year convection-permitting simulations. *Authorea Preprints*.

Huang, Y., Xue, M., Hu, X.-M., Martin, E., Novoa, H. M., McPherson, R. A., Perez, A. and Morales, I. Y. (2023b) Convection-permitting simulations of precipitation over the peruvian central andes: Strong sensitivity to planetary boundary layer parameterization. *Journal of Hydrometeorology*, **24**, 1969–1990.

Hwang, Y., Zhao, X., You, C.-H. and Li, Y. (2023) Climatological features of future mcss in convection-permitting climate models using cmip6 and era5 in the central united states. *Quarterly Journal of the Royal Meteorological Society*.

Iacono, M. J., Delamere, J. S., Mlawer, E. J., Shephard, M. W., Clough, S. A. and Collins, W. D. (2008) Radiative forcing by long-lived greenhouse gases: Calculations with the aer radiative transfer models. *Journal of Geophysical Research: Atmospheres*, **113**.

Ikeda, K., Rasmussen, R., Liu, C., Newman, A., Chen, F., Barlage, M., Gutmann, E., Dudhia, J., Dai, A., Luce, C. et al. (2021) Snowfall and snowpack in the western us as captured by convection permitting climate simulations: current climate and pseudo global warming future climate. *Climate Dynamics*, **57**, 2191–2215.

IPCC (2021) *Climate Change 2021 – The Physical Science Basis: Working Group I Contribution to the Sixth Assessment Report of the Intergovernmental Panel on Climate Change*. Cambridge University Press, 1 edn.

— (2022a) *Climate Change 2022 - Mitigation of Climate Change: Working Group III Contribution to the Sixth Assessment Report of the Intergovernmental Panel on Climate Change*. Cambridge University Press, 1 edn.

— (2022b) *Climate Change 2022 – Impacts, Adaptation and Vulnerability: Working Group II Contribution to the Sixth Assessment Report of the Intergovernmental Panel on Climate Change*. Cambridge University Press, 1 edn.

Jiménez, P. A., Dudhia, J., González-Rouco, J. F., Navarro, J., Montávez, J. P. and García-Bustamante, E. (2012) A revised scheme for the wrf surface layer formulation. *Monthly Weather Review*, **140**, 898–918.

Juckes, M., Taylor, K. E., Durack, P. J., Lawrence, B., Mizielinski, M. S., Pamment, A., Peterschmitt, J.-Y., Rixen, M. and Sénési, S. (2020) The cmip6 data request (dreq, version 01.00. 31). *Geoscientific Model Development*, **13**, 201–224.

Karki, R., Gerlitz, L., Schickhoff, U., Scholten, T., Böhner, J. et al. (2017) Quantifying the added value of convection-permitting climate simulations in complex terrain: a systematic evaluation of wrf over the himalayas. *Earth System Dynamics*, **8**, 507–528.

Kendon, E., Prein, A., Senior, C. and Stirling, A. (2021) Challenges and outlook for convection-permitting climate modelling. *Philosophical Transactions of the Royal Society A*, **379**, 20190547.

Kendon, E. J., Ban, N., Roberts, N. M., Fowler, H. J., Roberts, M. J., Chan, S. C., Evans, J. P., Fosser, G. and Wilkinson, J. M. (2017) Do convection-permitting regional climate models improve projections of future precipitation change? *Bulletin of the American Meteorological Society*, **98**, 79–93.

Kendon, E. J., Stratton, R. A., Tucker, S., Marsham, J. H., Berthou, S., Rowell, D. P. and Senior, C. A. (2019) Enhanced future changes in wet and dry extremes over africa at convection-permitting scale. *Nature communications*, **10**, 1794.

Knist, S., Goergen, K. and Simmer, C. (2020) Evaluation and projected changes of precipitation statistics in convection-permitting wrf climate simulations over central europe. *Climate Dynamics*, **55**, 325–341.

Komurcu, M., Emanuel, K., Huber, M. and Acosta, R. (2018) High-resolution climate projections for the northeastern united states using dynamical downscaling at convection-permitting scales. *Earth and Space Science*, **5**, 801–826.

Kouadio, K., Bastin, S., Konare, A. and Ajayi, V. O. (2020) Does convection-permitting simulate better rainfall distribution and extreme over guinean coast and surroundings? *Climate Dynamics*, **55**, 153–174.

Kukulies, J., Chen, D. and Curio, J. (2021) The role of mesoscale convective systems in precipitation in the tibetan plateau region. *Journal of Geophysical Research: Atmospheres*, **126**, e2021JD035279.

Kurkute, S., Li, Z., Li, Y. and Huo, F. (2020) Assessment and projection of the water budget over western canada using convection-permitting weather research and forecasting simulations. *Hydrology and Earth System Sciences*, **24**, 3677–3697.

Li, P., Furtado, K., Zhou, T., Chen, H. and Li, J. (2021) Convection-permitting modelling improves simulated precipitation over the central and eastern tibetan plateau. *Quarterly Journal of the Royal Meteorological Society*, **147**, 341–362.

Li, P., Moseley, C., Prein, A. F., Chen, H., Li, J., Furtado, K. and Zhou, T. (2020) Mesoscale convective system precipitation characteristics over east asia. part i: Regional differences and seasonal variations. *Journal of Climate*, **33**, 9271–9286.

Lind, P., Belušić, D., Christensen, O. B., Dobler, A., Kjellström, E., Landgren, O., Lindstedt, D., Matte, D., Pedersen, R. A., Toivonen, E. et al. (2020) Benefits and added value of convection-permitting climate modeling over fenno-scandinavia. *Climate Dynamics*, **55**, 1893–1912.

Lind, P., Belušić, D., Médus, E., Dobler, A., Pedersen, R. A., Wang, F., Matte, D., Kjellström, E., Landgren, O., Lindstedt, D. et al. (2023) Climate change information over fenno-scandinavia produced with a convection-permitting climate model. *Climate Dynamics*, **61**, 519–541.

Liu, C., Ikeda, K., Rasmussen, R., Barlage, M., Newman, A. J., Prein, A. F., Chen, F., Chen, L., Clark, M., Dai, A. et al. (2017) Continental-scale convection-permitting modeling of the current and future climate of north america. *Climate Dynamics*, **49**, 71–95.

Liu, C., Ikeda, K., Rasmussen, R., Dominguez, F., Prein, A. F., Dudhia, J. and Chen, F. (2022) An overview of two-decade-long convection permitting regional climate downscaling over the continental south america. In *American Geophysical Union Fall Meeting*. American Geophysical Union, Chicago, IL. URL: `https://agu.confex.com/agu/fm22/meetingapp.cgi/Paper/1115319`.

Lucas-Picher, P., Argüeso, D., Brisson, E., Tramblay, Y., Berg, P., Lemonsu, A., Kotlarski, S. and Caillaud, C. (2021) Convection-permitting modeling with regional climate models: Latest developments and next steps. *Wiley Interdisciplinary Reviews: Climate Change*, **12**, e731.

Marengo, J. A., Douglas, M. W. and Silva Dias, P. L. (2002) The south american low-level jet east of the andes during the 1999 lba-trmm and lba-wet amc campaign. *Journal of Geophysical Research: Atmospheres*, **107**, LBA–47.

Marengo, J. A., Soares, W. R., Saulo, C. and Nicolini, M. (2004) Climatology of the low-level jet east of the andes as derived from the ncep–ncar reanalyses: Characteristics and temporal variability. *Journal of climate*, **17**, 2261–2280.

Nakanishi, M. and Niino, H. (2009) Development of an improved turbulence closure model for the atmospheric boundary layer. *Journal of the Meteorological Society of Japan. Ser. II*, **87**, 895–912.

O'Neill, B. C., Tebaldi, C., van Vuuren, D. P., Eyring, V., Friedlingstein, P., Hurtt, G., Knutti, R., Kriegler, E., Lamarque, J.-F., Lowe, J., Meehl, G. A., Moss, R., Riahi, K. and Sanderson, B. M. (2016) The scenario model intercomparison project (scenariomip) for cmip6. *Geoscientific Model Development*, **9**, 3461–3482.

Paccini, L. and Stevens, B. (2023) Assessing precipitation over the amazon basin as simulated by a storm-resolving model. *Journal of Geophysical Research: Atmospheres*, **128**, e2022JD037436.

Potter, E. R., Fyffe, C. L., Orr, A., Quincey, D. J., Ross, A. N., Rangecroft, S., Medina, K., Burns, H., Llacza, A., Jacome, G. et al. (2023) A future of extreme precipitation and droughts in the peruvian andes. *npj Climate and Atmospheric Science*, **6**, 96.

Prein, A., Gobiet, A., Suklitsch, M., Truhetz, H., Awan, N., Keuler, K. and Georgievski, G. (2013) Added value of convection permitting seasonal simulations. *Climate Dynamics*, **41**, 2655–2677.

Prein, A. F., Langhans, W., Fosser, G., Ferrone, A., Ban, N., Goergen, K., Keller, M., Tölle, M., Gutjahr, O., Feser, F. et al. (2015) A review on regional convection-permitting climate modeling: Demonstrations, prospects, and challenges. *Reviews of geophysics*, **53**, 323–361.

Prein, A. F., Liu, C., Ikeda, K., Bullock, R., Rasmussen, R. M., Holland, G. J. and Clark, M. (2020) Simulating north american mesoscale convective systems with a convection-permitting climate model. *Climate Dynamics*, **55**, 95–110.

Prein, A. F., Liu, C., Ikeda, K., Trier, S. B., Rasmussen, R. M., Holland, G. J. and Clark, M. P. (2017a) Increased rainfall volume from future convective storms in the us. *Nature Climate Change*, **7**, 880–884.

Prein, A. F., Rasmussen, R. M., Ikeda, K., Liu, C., Clark, M. P. and Holland, G. J. (2017b) The future intensification of hourly precipitation extremes. *Nature climate change*, **7**, 48–52.

Qing, Y. and Wang, S. (2021) Multi-decadal convection-permitting climate projections for china's greater bay area and surroundings. *Climate Dynamics*, **57**, 415–434.

Rasmussen, K. L., Prein, A. F., Rasmussen, R. M., Ikeda, K. and Liu, C. (2020) Changes in the convective population and thermodynamic environments in convection-permitting regional climate simulations over the united states. *Climate Dynamics*, **55**, 383–408.

Roca, R. and Fiolleau, T. (2020) Extreme precipitation in the tropics is closely associated with long-lived convective systems. *Communications Earth & Environment*, **1**, 18.

Salio, P., Nicolini, M. and Zipser, E. J. (2007) Mesoscale convective systems over southeastern south america and their relationship with the south american low-level jet. *Monthly Weather Review*, **135**, 1290–1309.

Schumacher, R. S. and Rasmussen, K. L. (2020) The formation, character and changing nature of mesoscale convective systems. *Nature Reviews Earth & Environment*, **1**, 300–314.

Schumacher, V., Fernández, A., Justino, F. and Comin, A. (2020) Wrf high resolution dynamical downscaling of precipitation for the central andes of chile and argentina. *Frontiers in Earth Science*, **8**, 328.

Skamarock, W. C., Klemp, J. B., Dudhia, J., Gill, D. O., Liu, Z., Berner, J., Wang, W., Powers, J. G., Duda, M. G., Barker, D. M. et al. (2019) A description of the advanced research wrf model version 4. *National Center for Atmospheric Research: Boulder, CO, USA*, 145.

Sonuç, C. Y., Ünal, Y. and Incecik, S. (2023) Convection-permitting climate simulations with cosmo-clm over northwestern türkiye under the rcp8. 5 scenario. *International Journal of Climatology*, **43**, 3841–3858.

Stratton, R. A., Senior, C. A., Vosper, S. B., Folwell, S. S., Boutle, I. A., Earnshaw, P. D., Kendon, E., Lock, A. P., Malcolm, A., Manners, J. et al. (2018) A pan-african convection-permitting regional climate simulation with the met office unified model: Cp4-africa. *Journal of Climate*, **31**, 3485–3508.

Sun, X., Xue, M., Brotzge, J., McPherson, R. A., Hu, X.-M. and Yang, X.-Q. (2016) An evaluation of dynamical downscaling of central plains summer precipitation using a wrf-based regional climate model at a convection-permitting 4 km resolution. *Journal of Geophysical Research: Atmospheres*, **121**, 13–801.

549 Thompson, G., Field, P. R., Rasmussen, R. M. and Hall, W. D. (2008) Explicit forecasts of winter precipitation using an improved
550 bulk microphysics scheme. part ii: Implementation of a new snow parameterization. *Monthly Weather Review*, **136**, 5095–
551 5115.

552 Tiedtke, M. (1989) A comprehensive mass flux scheme for cumulus parameterization in large-scale models. *Monthly weather*
553 *review*, **117**, 1779–1800.

554 Vanden Broucke, S., Wouters, H., Demuzere, M. and van Lipzig, N. P. (2019) The influence of convection-permitting regional
555 climate modeling on future projections of extreme precipitation: dependency on topography and timescale. *Climate*
556 *Dynamics*, **52**, 5303–5324.

557 Vera, C., Baez, J., Douglas, M., Emmanuel, C., Marengo, J., Meitin, J., Nicolini, M., Nogues-Paegle, J., Paegle, J., Penalba, O.
558 et al. (2006) The south american low-level jet experiment. *Bulletin of the American Meteorological Society*, **87**, 63–78.

559 Wang, S. and Wang, Y. (2019) Improving probabilistic hydroclimatic projections through high-resolution convection-permitting
560 climate modeling and markov chain monte carlo simulations. *Climate Dynamics*, **53**, 1613–1636.

561 Wang, Y., Xiang, Y., Han, Z. and Song, L. (2023) Future extreme high-temperature risk in the beijing-tianjin-hebei urban ag-
562 glomeration of china based on a regional climate model coupled with urban parameterization scheme. *Theoretical and*
563 *Applied Climatology*, 1–14.

564 Wu, L. and Zheng, H. (2023) Regional climate effects of irrigation under central asia warming by 2.0° c. *Remote Sensing*, **15**,
565 3672.

566 Xu, Z., Han, Y., Tam, C.-Y., Yang, Z.-L. and Fu, C. (2021) Bias-corrected cmip6 global dataset for dynamical downscaling of the
567 historical and future climate (1979–2100). *Scientific Data*, **8**, 293.

568 Yang, X., Li, D., Yang, Z., Wu, K., Ji, L., Zhou, Z. and Lu, Y. (2023) Revealing historical observations and future projections
569 of precipitation over northwest china based on dynamic downscaled cmip6 simulations. *Frontiers in Earth Science*, **10**,
570 1090221.

571 Zaitchik, B. F., Rodell, M., Biasutti, M. and Seneviratne, S. I. (2023) Wetting and drying trends under climate change. *Nature*
572 *Water*, 1–12.

573 Zhao, M. (2022) A study of ar-, ts-, and mcs-associated precipitation and extreme precipitation in present and warmer climates.
574 *Journal of Climate*, **35**, 479–497.

575 Zhu, K., Xue, M., Zhou, B., Zhao, K., Sun, Z., Fu, P., Zheng, Y., Zhang, X. and Meng, Q. (2018) Evaluation of real-time convection-
576 permitting precipitation forecasts in china during the 2013–2014 summer season. *Journal of Geophysical Research: Atmo-*
577 *spheres*, **123**, 1037–1064.